Valence-electron energy loss near edges, truncated slabs, and junctions

J. Aizpurua*
Departamento de Física de Materiales, Facultad de Química, UPV/EHU, Apartado 1072, 20080 San Sebastián, Spain

A. Howie
Cavendish Laboratory, Madingley Road, Cambridge CB3 OHE, United Kingdom

F. J. García de Abajo
Departamento de CCIA, Facultad de Informática, UPV/EHU, Apartado 649, 20080 San Sebastián, Spain
(Received 21 September 1998; revised manuscript received 18 April 1999)

Valence losses in electron microscopy can be conveniently computed using classical dielectric excitation theory. In many practical situations, the presence of complex structures gives rise to the possibility of coupling between interface modes, surface modes, and edge modes. In the nonrelativistic case, the losses in such geometries can be calculated by taking a distribution of surface and interface points, each of which is associated with an interface charge. These charges interact self-consistently with each other as well as with the charge of the incident electron. Here, we have applied this boundary charge method to provide scanning transmission electron microscopy energy loss spectra near-edged structures such as truncated slabs and junctions formed by several media. We find the dominant modes associated with such systems and study their contribution to the characteristic energy loss functions. The significance of these excitations compared with the planar interface peaks is discussed in terms of the sample geometry with illustrations for the cases of an MgO cube and an Si/SiO_2 thin-film interface. [S0163-1829(99)00939-X]

I. INTRODUCTION

Electron energy loss spectroscopy (EELS) is a powerful tool to study the characteristics and nature of electron excitations in a solid. Spatially resolved EELS using fast electrons in scanning transmission electron microscopy (STEM) shows two types of loss depending on the nature of the initial electron states that are excited. Core electron excitations occur at very well-defined energies and have been successfully studied in terms of excitations from the different atomic levels corresponding to a specific atomic element. On the other hand, valence electrons give more intense spectral losses but their interpretation is much more difficult since these often have a collective nature connected not only to the composition of the material but also to the geometry of the sample under study. The dielectric theory, in which the media are described through a local dielectric function $\varepsilon(\omega)$ dependent only on the frequency, has however supplied an adequate basis for interpreting these excitations. The local approach, neglecting the momentum dependence of ε, can largely be applied in this kind of problem since very fast electrons in the scanning-beam transfer mainly rather small momenta. Following Ritchie's prediction of the surface plasmon excitation,[1] much work has been done on collective excitations associated with a particular geometry.[2] The aim has often been comparison between theoretical predictions and experimental loss spectra,[3] e.g., losses near a dielectric sphere[4] or Ag spherical particles.[5] STEM experiments in easily damaged materials such as AlF_3 yielded loss spectra from cylindrical holes and stimulated analytical solutions for appropriate geometry.[6] Losses from colloidal dispersions of small spherical precipitates were also found[7] and interpreted in terms of effective medium theory. Analytical studies of modes and plasmon frequencies in cubes, rectangular particles and wedges have also been made by several authors.[8–10] As the geometry involved in real problems becomes more complicated, a mixture of both analytical and computational work is required in order to solve systems such as a sphere coupled to a plane,[11] a hemisphere,[12] a channel,[13] or a wedge.[14] When the number of particles, or of different media, or the difficulty of the geometry itself do not allow an analytical solution, other computational techniques are necessary to deal with the problem. Fuchs[15] determined the normal modes of a cube by distributing dipoles over a solid, selfconsistently interacting with one another. Ouyang and Isaacson[16] developed a formalism to deal with inhomogeneous dielectric systems that was based on solving Poisson's equation with a distribution of surface charge density at every interface separating two different media and applied it to calculate the energy losses of a spherical particle lying on a thin film.[17] A similar approach was followed to calculate electron energy losses near both translationally invariant and axially symmetric targets with otherwise arbitrary shape.[18] In fact, this paper can be understood as a continuation of this previous work since all the formalism used here was already explained there in more detail (apart from slight changes in notation which are noted here when they arise). Here we study further the application of this general formalism to a number of practical situations in STEM. The interfaces and so the surface charge densities can be discretized in a convenient way in order to solve a self-consistent integral equation, which involves the surface charge density distribution. As an example of the power of the technique, we provide simulations for a variety of cases not studied previously due to the complexity of the geometry or to the number of media involved. These calculations are exact for such con-

figurations, but we also include some approximate characteristic energy loss functions that refer the spectrum of losses to a few dominant modes that are strongly excited by the incoming beam. These approximate functions may be found useful by experimentalists in a certain number of cases where a complicated spectrum of losses occurs. The detailed description of the loss spectra must of course ultimately depend on the exact numerical computation but the approximate function can throw light on the nature and intensity of the losses found. In this spirit, different features of the spectrum of modes and losses arising near the end of a truncated slab are simulated to investigate the influence of slab thickness on the mode coupling for edges and walls. A real system that shows such geometrical features is the MgO cube whose excitations by STEM electrons have been studied by Marks,[19] Cowley,[20] and Milne and Echenique[21] among others. Loss spectra for different trajectories are shown and explained in terms of bulk and surface losses. Using the formalism presented previously[18] and summarized more briefly here, we are able to study in a systematic way the losses in these systems even for trajectories close to the edges. We can also study complex junctions where several media meet at a fixed point or line. It is possible to simulate maps of energy losses for such complex systems resembling the energy selected loss images. Furthermore, another case of interest that shows coupling between edges and mixes several media is the system formed by a junction of Si and SiO_2 in a slab surrounded by vacuum. Previous calculations on this system[22,23] were based on a Si-SiO_2 planar interface approximation and suggested the presence of a 1-nm-thick layer of SiO at the interface in order to explain the observed magnitude of the interface plasmon peak. The importance of retardation effects in determining the peak position was also noted. These calculations did not take into account the influence of the thickness of the slab on the loss spectrum, i.e., the top and bottom surfaces and the corners forming the edges, something we remedy in this paper. We have to point out that all the calculations performed here ignore retardation and radiation effects, that is, we are dealing within a nonrelativistic approximation in which Poisson's equation for each Fourier component of frequency ω is solved numerically for different cases of interest. As the velocity of electrons in the scanning beam is of the order of $c/2$, this approximation will be more accurate for small enough samples and particles and trajectories close enough to the interface. Beyond these limits, one should introduce retardation to get accurate quantitative values. The boundary charge numerical method has been recently extended to include retardation effects by solving Maxwell's equations rather than Poisson's equations.[24] All the examples treated here involve small impact parameters so that retardation effects may not be too serious. In some cases (noted below), Cherenkov radiation or transition radiation may occur and is not included in our nonrelativistic treatment. Nevertheless the nonrelativistic boundary charge method shows promise as a tool to treat real systems in STEM configurations. As an application of this numerical method to cases of practical interest in STEM, we analyze, first, the case of the edge and the truncated slab as an example of a complex two-media geometrical system and second, the cases of the *T* and *I* junctions where the complexity arises from the number of media involved in the system as well as from the sharp boundaries which occur in these structures.

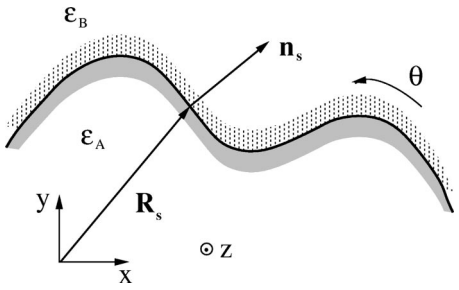

FIG. 1. Schematic representation of an interface separating media ε_A and ε_B with invariance along the z axis. The unit vector $\mathbf{n}_s$ normed to the interface at position $\mathbf{s}$ points towards medium ε_B. The arrow indicates the sense of increasing parameter θ.

II. BASIC THEORY

We briefly outline in this section the theoretical basis, which allows systematic calculation of the modes and losses for an arbitrarily shaped object. The theory for the nonretarded case has already been presented in detail[18] and we merely summarize it here for completeness.

A. The boundary charge method

The key to deal with losses in arbitrary objects is given by the possibility of writing the potential and electric field all over the space in terms of the surface charge density induced by an external field (produced by the incoming electron in this case) at the interfaces separating the different media. The surface charge density $\sigma(\mathbf{s},\omega)$ at each interface point $\mathbf{s}$ interacts consistently with the charge at the other points $\mathbf{s}'$, as well as with the external field frequency component $\nabla\phi^{\mathrm{ext}}(\mathbf{s},\omega)$, which in Ref. 18 was denoted by $\nabla\phi^{\infty}(\mathbf{s},\omega)$, produced by the passing electron. From Poisson's equation the self-consistency expression based on the surface charge density leads to

$$\Lambda(\omega)\sigma(\mathbf{s},\omega)=\mathbf{n}_{\mathbf{s}}\cdot\nabla\phi^{\mathrm{ext}}(\mathbf{s},\omega)-\int d\mathbf{s}'\frac{\mathbf{n}_{\mathbf{s}}\cdot(\mathbf{s}-\mathbf{s}')}{|\mathbf{s}-\mathbf{s}'|^3}\sigma(\mathbf{s}',\omega), \tag{1}$$

where

$$\Lambda(\omega)=2\pi\frac{\varepsilon_B(\omega)+\varepsilon_A(\omega)}{\varepsilon_B(\omega)-\varepsilon_A(\omega)}, \tag{2}$$

and

$$\phi^{\mathrm{ext}}(\mathbf{r},\omega)=\int d\mathbf{r}''\frac{\rho^{\mathrm{ext}}(\mathbf{r}'',\omega)}{\varepsilon(\mathbf{r}'',\omega)|\mathbf{r}-\mathbf{r}''|}. \tag{3}$$

The dielectric responses are described in terms of an arbitrary function of space $\mathbf{r}''$ and frequency ω, $\varepsilon(\mathbf{r}'',\omega)$, which denotes the local dielectric function at the point $\mathbf{r}''$ (either ε_A or ε_B in the simplest case). $\varepsilon_A(\omega)$ and $\varepsilon_B(\omega)$ are the dielectric functions of the two media surrounding each interface point $\mathbf{s}$ as shown in Fig. 1, and $\rho^{\mathrm{ext}}(\mathbf{r}'',\omega)$ denotes the Fourier component of the external charge density associ-

ated with the electron beam that is assumed to move in a material of dielectric function $\varepsilon(\omega)$. As can be observed in Eq. (1), the surface charge density can be obtained through a self-consistent integral equation involving all the interface points. In order to deal with practical cases and nonstandard geometries the integration can be converted to a matrix operator where the surface charge points are discretized and conveniently distributed, depending on the local interface shape and its closeness to the beam. In addition to this, if the system shows some kind of translational or rotational geometrical symmetry the integral equation simplifies and turns into a one-dimensional problem, when appropriately projected over the invariant coordinate z. We deal in this paper with objects invariant along the z axis, which takes account of the main features of the edges, truncations, and junctions present in many real systems such as cubes or thin films composed of two different components. In this way, the parametrization of the interface depends only on one parameter θ, and can be performed in the XY plane as shown in Fig. 1. If we project Eq. (1) over the Fourier transformed component q of the invariant real coordinate z, we get

$$\Lambda(\omega)\sigma_q(\theta,\omega)=f_q(\theta,\omega)+\int d\theta' F_q(\theta,\theta')\sigma_q(\theta',\omega), \tag{4}$$

where the surface charge density $\sigma_q(\theta,\omega)$ depends only on the parameter θ. The explicit expression for the q component of the external term is

$$f_q(\theta,\omega)=\mathbf{n}_s(\theta)\cdot\nabla\phi_q^{\mathrm{ext}}[\mathbf{R}_s(\theta),\omega] = \int \frac{d\mathbf{R}''}{\varepsilon(\mathbf{R}'',\omega)} H_q(\mathbf{R}'',\theta)\rho_q^{\mathrm{ext}}(\mathbf{R}'',\omega), \tag{5}$$

where

$$H_q(\mathbf{R}'',\theta)=2|q|K_1[|q||\mathbf{R}''-\mathbf{R}_s(\theta)|]\mathbf{n}_s(\theta)\cdot\frac{[\mathbf{R}''-\mathbf{R}_s(\theta)]}{|\mathbf{R}''-\mathbf{R}_s(\theta)|}. \tag{6}$$

$\mathbf{R}''=(x'',y'')$ is the projection of the position vector over the XY plane perpendicular to the invariant axis z, $\mathbf{n}_s(\theta)$ the unit vector normal to the interface at each point, and $K_1[x]$ is a modified Bessel function of first order. When the trajectory crosses several media, $\varepsilon(\mathbf{R}'',\omega)$ depends on the particle position $\mathbf{R}''$, and the integral in Eq. (5) has to be broken into the different regions the electron is crossing. Otherwise, when the medium surrounding the incoming particle does not change, it can be directly expressed as $\varepsilon(\omega)$. The self-consistent-induced term or interaction matrix is given by

$$F_q(\theta,\theta')=\sqrt{x_s'(\theta')^2+y_s'(\theta')^2}H_q[\mathbf{R}_s(\theta'),\theta], \tag{7}$$

where the prime denotes differentiation with respect to the parameter θ'.

When solving the integral equation for the surface charge density in expression (4) by means of a convenient discretization of the whole interface present in a system, the integral equation turns into an algebraic system that can be expressed in a matrix form:

$$\Lambda(\omega)[\sigma_q]_i=[f_q]_i+\sum_j [F_q]_{i,j}[\sigma_q]_j, \tag{8}$$

where $[\sigma_q]_i=\sigma_q(\theta_i,\omega)$ is the surface charge density corresponding to the ith point of the surface parametrization, $[f_q]_i=f_q(\theta_i,\omega)$ is the q component of the external field produced by the incoming electron at the ith position and $[F_q]_{i,j}=F_q(\theta_i,\theta_j)\Delta\theta_j$ is the q component of the interaction between the ith and jth surface points of the parametrization (the interaction matrix). In this process of discretization, a sufficient number of points must be considered in order to get convergence in the results. In the nanometric scale, typically it was found necessary to use around 100 surface points. These were generally concentrated in the regions of interest of smallest curvature and closest to the electron beam path with a smaller number of points at greater distances. The number of points needed for convergence of the computed loss spectrum and their maximum distance from the electron beam were found by trial and error. It is important to point out that this method separates clearly the geometry of the system (given by $[F_q]_{i,j}$), the composition (given by Λ, which depends on the pair ε_A and ε_B surrounding every interface) and the strength of the induced charge density (given by $[f_q]_i$, which depends mainly on the impact parameter of the incoming electron).

B. Dominant interface modes

The eigenmodes for a given geometrical system can be easily obtained from Eq. (8) by neglecting the external term $[f_q]_i$ and setting the determinant of the interaction matrix $[F_q]_{i,j}$ to zero, which is the condition for the charge density to exist without an external field. Apell *et al.*[25] found that these modes fulfill interesting sum rules, which apply in such situations. Once the modes are calculated, they are excited with different weights depending on the particular conditions of the trajectory.

For a two-media situation it is possible to calculate a spectrum of modes as a standard eigenvalue problem for the $[F_q]_{i,j}$ matrix, which depends only on the geometry of the structure and not on the two particular media involved.[18] If we denote by $2\pi\lambda_q^k$ the eigenvalues of the interaction matrix $[F_q]$, associated with a corresponding eigenvector $[\sigma_q]^k$, the equation for the mode of this particular surface charge density can be expressed as

$$2\pi\lambda_q^k[\sigma_q]_i^k=\sum_j [F_q]_{i,j}[\sigma_q]_j^k, \tag{9}$$

where i,j labels the matrix elements and the vector components. The interface modes have to be labeled with two parameters: q (wave vector along the symmetry axis) and k (a mode number normal to this axis).

The set of eigenvectors $[\sigma_q]^k$ form a complete basis whose orthogonality properties are derived from[16]

$$\int d\mathbf{s}\int d\mathbf{s}'\frac{\sigma^i(\mathbf{s})\sigma^j(\mathbf{s}')^*}{|\mathbf{s}-\mathbf{s}'|}=\delta_{ij}. \tag{10}$$

This allows us to project the expression for the external term in terms of these eigenvectors as

$$\mathbf{n_s}\cdot\nabla\phi_q^{\rm ext}(\mathbf{s},\omega)=\sum_k f_q^k(\omega,b)\sigma_q^k(\mathbf{s}), \tag{11}$$

where $f_q^k(\omega,b)$ is the projection of the external term f_q over the k eigenvector $\sigma_q^k(\mathbf{s})$, and depends on the particular trajectory described via the impact parameter b.

If there are only two media forming the system, the eigenvalue λ_q^k is straightforwardly related with the parameter $\Lambda(\omega)$ through

$$\Lambda(\omega)-2\pi\lambda_q^k=0, \tag{12}$$

which gives account of the k-mode position (ω_k) for every value of q. In terms of the two local dielectric functions ε_A and ε_B, Eqs. (2) and (12) give

$$(1+\lambda_q^k)\varepsilon_A+(1-\lambda_q^k)\varepsilon_B=0, \tag{13}$$

which is the mode equation for translationally invariant interfaces separating two different media.

The total interface charge density $\sigma_q(\mathbf{s},\omega)$ can be obtained as a sum over all the modes present in the geometrical system, weighted with the external term $f_q^k(\omega,b)$

$$\sigma_q(\mathbf{s},\omega)=\sum_k \frac{f_q^k(\omega,b)}{[\Lambda(\omega)-2\pi\lambda_q^k]}\sigma_q^k(\mathbf{s}). \tag{14}$$

In principle, the exact solution of the interface charge density consists of the sum over all the eigenmodes, but in practical STEM configurations only some dominant modes are significantly excited and play an important role in the spectrum of energy loss. One of the aims of this paper is, therefore, to detect and deal with these dominant modes in complex configurations formed by the coupling of edges and junctions.

C. Characteristic energy loss functions

In a general formulation of the problem, the energy loss probability and hence, the excitation probability for a dielectric can be obtained by the action of the retarding field due to the induced interface charge density $\sigma(\mathbf{s},\omega)$ at the position of the incoming electron. The explicit expression for the loss probability is given by a weighted sum over different modes (labeled k) associated with the different contributions of the induced surface charge density $\sigma_q^k(\mathbf{s},\omega)$ in Eq. (14). For a two media problem, one can write the excitation probability for a dielectric system $\Gamma_q^{\rm boundary}$ as a weighted sum over different modes:

$$\Gamma_q^{\rm boundary}=\frac{1}{v^2}\sum_k {\rm Im}\{-g_q^k(\omega)\Gamma_q^k\}. \tag{15}$$

$g_q^k=2/[\varepsilon_A(1+\lambda_q^k)+\varepsilon_B(1-\lambda_q^k)]$ gives the mode position as noted in the previous section and Γ_q^k, which gives the contribution of the k mode is proportional to $\sigma_q^k(\mathbf{s})$ and f_q^k. For trajectories parallel to the invariant direction, conservation of energy and momentum means that only one value $q=\omega/v$ is relevant in the loss spectrum, v being the velocity of the fast electron. For perpendicular trajectories, there has to be an integration over q, which roughly speaking extends up to values of order $|q|=1/b$ where b is the impact parameter measured from the nearest interface point. This decrease in the probability of excitation for larger values of q arises naturally in the formalism due to the nature of the Coulomb interaction which introduces a dependence proportional to qb in the argument of the Bessel function $\sim K_1[qb]$ [see Eq. (6)]. If we now set $\alpha_k=1+\lambda^k/2$ and $A_k(\omega,b)=(2/\pi)\Gamma_k$, we find a simple expression for the excitation probability $dP/d\omega$ in a two-component system

$$\frac{dP}{d\omega}=\frac{2e^2}{\pi\hbar v^2}\sum_k^n A_k(\omega,b){\rm Im}\left[\frac{-1}{\alpha_k\varepsilon_A+(1-\alpha_k)\varepsilon_B}\right], \tag{16}$$

where α_k gives the position of the kth mode in terms of its eigenvalue λ^k strongly dependent on the shape of the sample, and $A_k(\omega,b)$ is the weight of the mode under the particular circumstances of excitation (impact parameter and size of the sample). In principle, the sum over the modes involves as many modes as the number of interface points in the parametrization, but in practice, for a real system such as an edge or a truncation, it is sufficient to take the dominant modes which can be efficiently excited and act back at the incoming electron, i.e., those with large values of $A_k(\omega,b)$. As indicated in later sections, an adequate approximation to the loss spectrum can often be obtained by including only 3 or 4 modes.

III. ISOLATED EDGE

In many practical situations, the presence of sharp edges is a prominent feature that cannot be neglected when an accurate study of the electron energy losses is required. We try to show here quantitatively the influence of the presence of an edge in the spectra of losses. In all the cases, the edges are considered very sharp compared to the distance of the beam. Therefore, the shape of the apex does not introduce an extra dependence in the mode frequency position which is given effectively by the junction of two straight walls.

A. Drude-like metallic edge

As pointed out in the previous section, we assume several mode contributions to describe the whole spectrum of losses. In the case of a sharp edge, it was found that the discrete distribution of surface modes corresponds to the values $\alpha_j=0.30$ (symmetric), 0.70 (antisymmetric), 0.34 (symmetric), 0.63 (antisymmetric), . . . , together with a cluster of values around 0.5 (planar surface plasmon).[18] It should be noted that for subsequent convenience with the more complex T and I junctions discussed below, the discretization procedure used here for the isolated edge is slightly different than the one previously employed.[18] Here, all the points lie on the two intersecting planes forming the edge. Although there is no point at the actual intersection of the two planes, since the surface normal is not well defined there, points if necessary can be taken arbitrarily close to the intersection by working with finer and finer mesh scales. With this slightly different procedure, the α values for the edge modes become slightly different, but the changes in the loss spectra are extremely small.

Although all the modes belong to the edge geometry, only some of them are noticeably excited when the electron impinges on such a structure. Figure 2 shows the spectrum of losses for a 100-keV electron impinging with an impact pa-

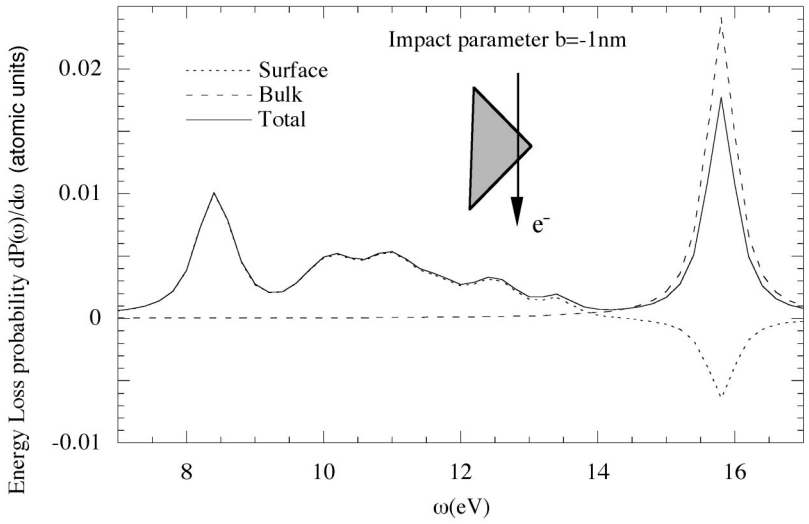

FIG. 2. Total energy loss probability for a 100-keV electron impinging on a sharp edge of Al. The impact parameter is 1nm inside the edge. Bulk and surface contributions to the losses are also plotted.

rameter of -1 nm on a single 90° edge of aluminum, characterized by a Drude-like dielectric function $\varepsilon_A = 1 - \omega_p^2/[\omega(\omega + i\gamma)]$ with plasma frequency $\omega_p = 15.8$ eV and damping $\gamma = 0.5$ eV surrounded by vacuum $\varepsilon_B = 1$. The minus sign for the impact parameter denotes a trajectory inside the material measured from the vertex of the edge. For such a case, it is clear that together with the bulk peak at 15.8 eV, the main contribution to the spectrum of losses is the peak at 8.3 eV, corresponding to $\alpha = 0.30$, which denotes the edge peak corresponding to the first symmetric surface mode at the edge. The contribution of the pure planar mode $(\omega_p/\sqrt{2})$ due to the walls of the edge is also present at 11.2 eV. For a beam passing normally through an edge, at a distance b from the vertex of the edge, the path travelled inside the material is $L = 2|b|$, and after integrating over the different q components and total path, the approximate energy loss probability becomes

$$\frac{dP}{d\omega} = \frac{2e^2}{\pi\hbar v^2} L \left\{ A_o \, \mathrm{Im}\left[\frac{-1}{\varepsilon_A}\right] + A_1 \, \mathrm{Im}\left[\frac{-1}{0.5\varepsilon_A + 0.5\varepsilon_B}\right] + A_2 \, \mathrm{Im}\left[\frac{-1}{0.3\varepsilon_A + 0.7\varepsilon_B}\right] \right\}, \tag{17}$$

where $A_k = A_k(b,\omega)$, $(k = 0,1,2)$ depend on the impact parameter b and give the weight of the three main excitations in the loss probability whose α_k values have been explicitly written. In the case of a penetrating trajectory, the first mode to be taken into account is the bulk mode characterized by $\alpha_o = 1$. The second important feature that arises naturally from the formalism is the pure planar mode characterized by $\alpha_1 = 0.5$ and finally the main mode associated with the charge density oscillations near the edge, which are described by $\alpha_2 = 0.30$. As pointed out above, there are more modes associated with the edge (symmetric and antisymmetric ones oscillating all around the edge[18]), but since this latter is the one which dominates the spectrum of losses, it is enough to consider it alone to show the main features of the losses produced by the edge. In order to account for the additional background in Fig. 2 given by the exact calculations, one should certainly include another pair of modes, but this is an extreme case of free electron response with relatively small damping when the contribution of each mode is more easily detected. For a practical material, such as that shown in the next section, this reductionist approximation describes most of the features of a given spectrum. This will be the spirit of the following approximations in the characteristic energy loss functions of complex structures. It is interesting to stress here that the values α_k giving rise to the surface modes are not as arbitrary as one might think at first sight. In fact, although there is a considerable spread of modes $(0 < \alpha_k < 1)$ all along the spectrum, it is noticeable that the most prominent wedge mode position shows a systematic tendency to increase with the wedge angle or filling fraction getting close to $\sim 1/4$ in the case of a perfectly straight 90° edge.

The weight of every mode A_k depends only on the impact parameter b with respect to the apex of the edge. The coefficients do not follow any known analytical dependence as a function of the impact parameter. For the particular case shown in Fig. 2, however, the coefficients can be approximated as

$$A_o = \ln(k_c v/\omega) - \frac{200\ \mathrm{nm}}{L}[1 - e^{(-2|b|\omega/v)}],$$

$$A_1 = \frac{300\ \mathrm{nm}}{L}[1 - e^{(-2|b|\omega/v)}], \tag{18}$$

and

$$A_2 = 650[e^{(-10|b|\omega/v)}],$$

with an accuracy of 10% in the estimate of the functional dependence. For the case of a trajectory perpendicular to the axis of symmetry as shown in the inset of Fig. 2, the edge mode $(\alpha_2 = 0.30 \Rightarrow \omega \sim 0.53\omega_p)$ decreases very strongly in intensity with increasing distance $|b|$ from the edge $(\sim e^{(-10|b|\omega/v)})$ and the planar surface mode intensity increases more slowly $(\sim e^{(-2|b|\omega/v)})$ to a fixed value. The bulk mode also increases in intensity with distance from the edge, since the beam travels through a longer path inside the material. For such penetrating trajectories, this peak is corrected by a term that follows an analogous dependence to the

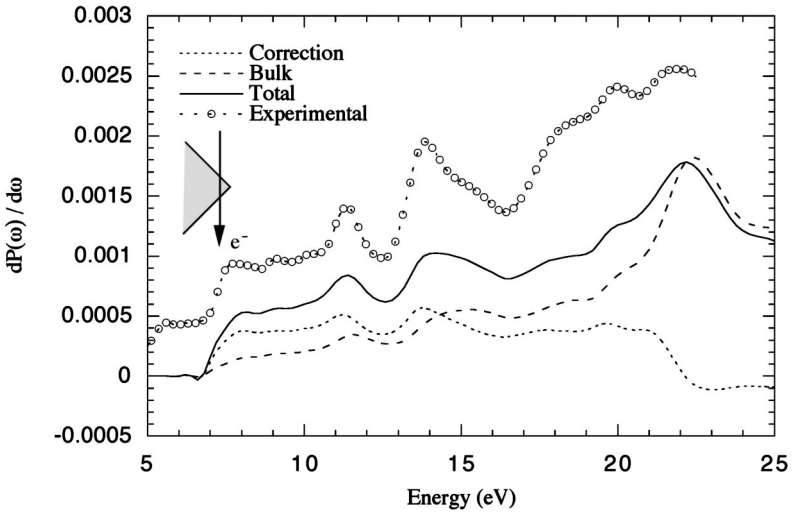

FIG. 3. Total energy loss probability for a 100-keV electron impinging on an MgO edge as shown in the inset. The impact parameter is 1 nm inside the edge. Bulk and surface contributions to the losses are also plotted.

planar surface contribution with contrary sign (Begrenzung effect: the excitation of new surface modes decreases the intensity of the bulk peak).

B. MgO edge

This edge geometry was also studied for the more practical case of MgO cubes,[26] which show sharp edges. Although the peaks cannot be so precisely associated with a particular geometrical feature as in the case of a simple metal, similar conclusions were reached. The MgO sample considered is in fact infinite in the z direction normal to Fig. 3 and the distance from the apex to the farthest surface point is taken to be 100 nm in the computation. Since we are concerned with the effect of the edge, the coupling between parallel sides of the cube is not included in this particular calculation, but this can be considered a good approximation for the large size of cube studied here (several hundreds of nm) where this coupling is absolutely negligible. The procedure to calculate the spectrum of losses for the case of an MgO edge is analogous to the one presented above for the metallic edge, but in this case, the frequency-dependent dielectric function is derived from the bulk loss function in the same material extracted from energy loss data after deconvolution. In Fig. 3, we present both the STEM observed energy loss spectrum and, for the identical trajectory, the total simulated energy loss probability $dP(\omega)/d\omega$, which agrees in absolute terms to a factor of about 0.7. Together with the bulk loss at 22.5 eV, the enhancement of the low-energy peaks at 11 and 14 eV can only be explained in terms of the edge mode associated with this structure. As in the case of the metallic edge the correction introduced by the surface features influences the spectrum by enhancing the weight of the peaks more sensitive to the edge (low-energy peaks) and on the other hand, by decreasing smoothly the weight of the bulk loss in a Begrenzung-like effect associated with the edge and walls as mentioned above. Equations (17) and (18) also fulfil for this case with $\varepsilon_A=\varepsilon_{\mathrm{MgO}}$ and $\varepsilon_B=1$. The planar contribution (20 eV) associated to $\alpha_1=0.5$ is not so strong in this case due to the fact that the trajectory is very close to the apex of the edge [see approximate functional dependence for A_1 in Eq. (18)]. Also the bulk peak does not mask the surface and edge correction at such impact parameters. In any case, the main geometrical uncertainty is the precise value of the impact parameter that can change the total weight of the loss probability due to a different contribution arising from the bulk losses. The simulation does not reproduce the excitations observed in the band gap which must arise either from defects or from relativistic effects.

IV. COUPLED EDGES: TRUNCATED SLAB

A. Interface modes

Another case of interest from the practical point of view is the truncated slab that can be considered as the junction of two edge structures. A major parameter then involved is the slab thickness d. In Fig. 4 the modes of a truncated slab depending on the dimensionless parameter qd are shown, being q the momentum component in the direction parallel to the axis of symmetry z as shown in Fig. 1. The dielectric response function ε is assumed to be a Drude-like function with no damping ($\gamma=0$). For very thick slabs ($qd>1.5$), the limit of the isolated edge is obtained with the presence of well-defined modes ($\omega\sim 0.53\omega_p, 0.63\omega_p, \ldots, 0.80\omega_p$ and a concentration of modes close to the value $\omega_p/\sqrt{2}$). As the thickness of the slab decreases, the modes start to couple giving rise to a spread of allowed values. As in the case of the isolated edge, some of these modes are more likely to be excited depending on the particular features of the electron trajectory, which couples better to some particular density charge distribution with a large amplitude nearby. It is also possible to plot the charge density oscillations associated with every particular mode since the eigenvectors of the interaction matrix $[F_q]$ in expression (7) are the contribution to the surface charge density corresponding to each mode.

In Fig. 5 the surface charge density $\sigma_q(\mathbf{s},\omega)$ for six dominant modes in the case $qd=0.6$ (which corresponds to $d\sim 10$ nm in a Drude-like aluminum for a momentum transfer typical of STEM $q=\omega/v$) are shown all along the boundaries of the truncation of the slab. There are three slab-symmetric modes [Figs. 5(a), 5(c), and 5(e)] corresponding to $\omega=0.40\omega_p$, $\omega=0.54\omega_p$, and $\omega=0.83\omega_p$ which come from the lower branches of the edge coupling, and three slab-antisymmetric modes [Figs. 5(b), 5(d), and 5(f)] corresponding to $\omega=0.86\omega_p$, $\omega=0.55\omega_p$, and $\omega=0.82\omega_p$,

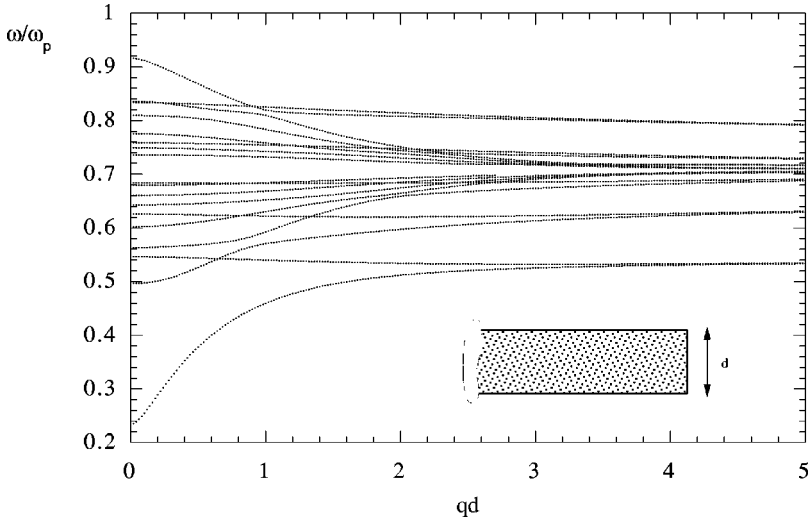

FIG. 4. Spectrum of modes for the truncated end of a metallic slab as shown in the inset as a function of the dimensionless parameter qd. The dielectric function of the slab is characterized by a plasma frequency ω_p.

which comes from the upper branch of the coupling (see Fig. 4 for $qd=0.6$). On the other hand, it is also possible to determine the nature of the different modes in terms of the symmetry with respect to the bisector of the isolated edge itself. Those modes whose frequency is smaller than the planar interface mode, i.e., $\omega<\omega_p/\sqrt{2}$ are edge-symmetric modes, whereas the edge-antisymmetric modes are found for frequencies greater than the planar interface mode, i.e., $\omega>\omega_p/\sqrt{2}$. As the slab becomes thinner, the coupling of edges and walls is enhanced as can be checked in Fig. 4, and the values of the resonance frequencies are clearly shifted up and down. In any case, the interface charge density associated with each mode follows the same scheme as that for $qd=0.6$ and the nature of each mode can be explained in terms of slab-symmetry and edge-symmetry.

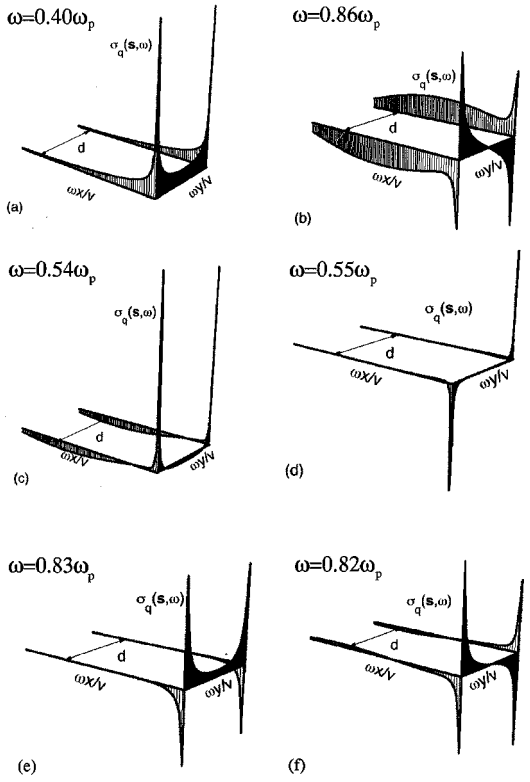

FIG. 5. (a), (b), (c), (d), (e), and (f) show, respectively, the surface charge density $\sigma(\theta)$ of the first modes at a truncated slab as a function of the dimensionless coordinates $x\omega/v$ and $y\omega/v$ for the case $qd=0.6$. Notice that there are edge-symmetric and antisymmetric modes and slab-symmetric and antisymmetric ones.

In Figs. 6(b), 6(c), and 6(d) we have calculated the loss spectra for three different cases of truncated slabs of aluminum, when the electron trajectory is parallel to the axis of symmetry at different positions outside the slab as shown in Fig. 6(a). The trajectories have been labeled from 0, the center of the truncation, to 2, the furthest trajectory from the edge of the truncation. In the first case [Fig. 6(b)] the thickness of the slab is 20 nm and only two clear excitations can be observed. The distance between the two edges is enough to excite only the modes of the pure planar case and the isolated edge separately. The isolated edge mode ($\sim\sqrt{0.3}\omega_p=8$ eV) is clearly excited when the beam is close to it (label 1) since the interaction between walls is not noticeable. For trajectories close to the middle of the truncation (label 0) the pure planar mode ($\omega_p/\sqrt{2}=11.2$ eV) is clearly excited. For trajectories closer to the edge, the planar loss decreases as the edge loss rises (Begrenzung effect). This situation corresponds in aluminum to the excitation of modes at $qd\sim1.5$ where the isolated edge accounts on its own for all the excitations present in the spectrum of losses. As the truncated slab is made thinner, the walls and edges are closer and the coupling make the modes split up all over the spectrum. In the second case [Fig. 6(c)], corresponding to $qd\sim0.6$, the main excited peak belongs to a low-energy coupled mode ($0.40\omega_p=6.3$ eV). This peak corresponds to the first slab-symmetric mode plotted in Fig. 5(a) and has the most intense excitation just in the middle of the truncation (label 0). There is a slab anti-symmetric mode at $0.54\omega_p$ (8.53 eV), which is also excited near the edge (label 1). The pure planar mode is still excited but with a lower intensity since the proximity of the edge boundaries and the Begrenzungs effect do not allow it to be excited in this region. In the third case [Fig. 6(d)], for a 5-nm slab, the low energy peak is excited at a still lower energy ($0.28\omega_p=4.5$ eV) due to the stronger coupling among interfaces which corresponds to $qd\sim0.2$ in the spectrum of modes of Fig. 4. From these examples, it is possible to conclude that the coupling of edges and walls is relevant for slab thicknesses of less than the parameter v/ω_p, which is 15 nm for the case 100 keV electrons impinging on aluminum.

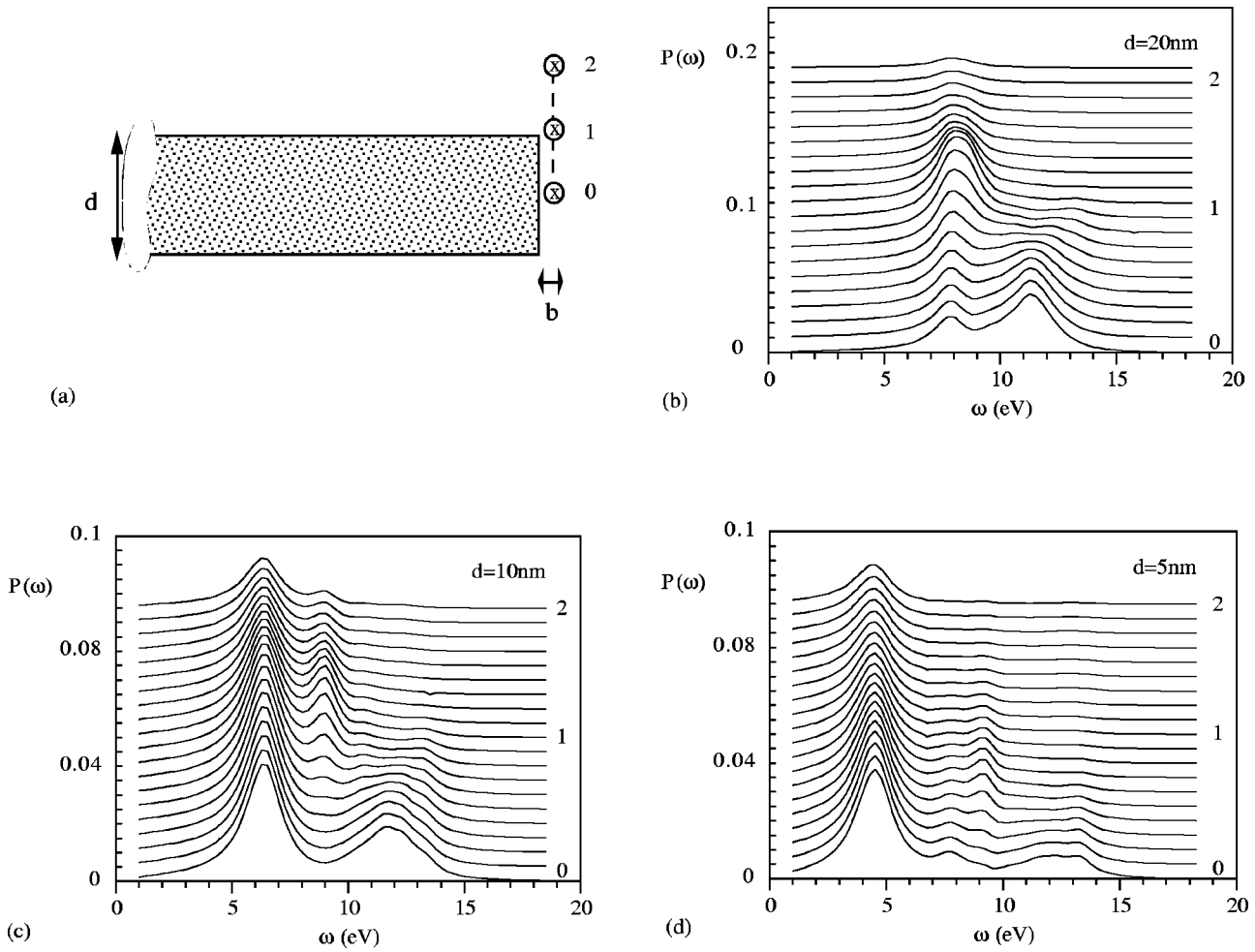

FIG. 6. (a) Schematic representation of a truncated slab with several trajectories marked from 0 (close to the center of the truncation) to 2 (far away from the edge of the truncation). (b),(c),(d) Spectra of losses for aluminum slabs ($\omega = 15.8$ eV and damping $\gamma = 1.35$ eV) of different thickness (20, 10, and 5 nm, respectively) when the electron travels parallel to the axis of symmetry at the positions shown in (a). The impact parameter is 2 nm in all the cases and d is the slab thickness.

B. Influence of specimen thickness in EELS

The simulations and observations of energy losses when the beam travels perpendicular to the axis of symmetry gives another possibility to study the edge effect on the loss spectra. In Fig. 7, the spectrum of losses normalized to the slab thickness d is shown for such a trajectory and different values of d. The impact parameter b is 2 nm outside the slab measured from the truncation. We compare the spectrum of losses for $d = 20$, 50, 100, and 200 nm with the pure planar case ($d \rightarrow \infty$). For the thickest slab, it is clear that the planar expression is adequate to describe the features of the spec-

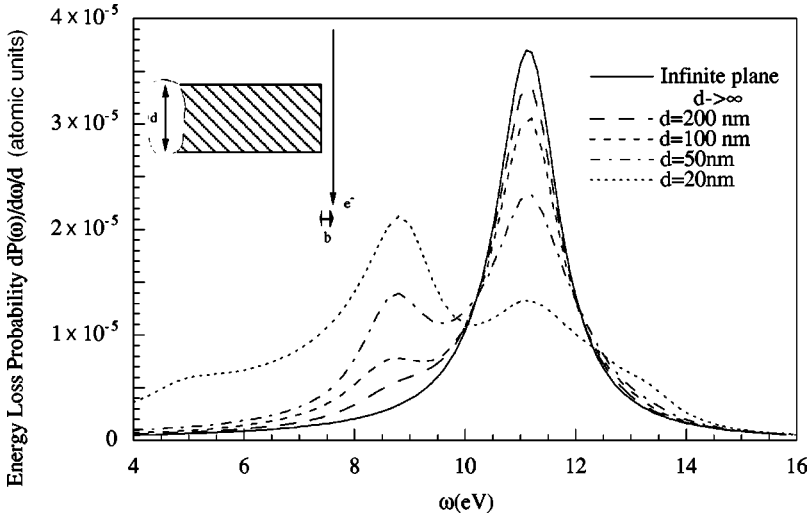

FIG. 7. (a) Energy loss probability for Al slabs of different thickness d (200, 100, 50, and 20 nm, respectively) when the electron travels perpendicular to the axis of symmetry as shown in the inset compared with the pure planar interface ($d \Rightarrow \infty$) under the same circumstances. The impact parameter b is 2 nm outside the truncation. Notice that the surface planar excitation is recovered for thick enough slabs.

trum since the edge region is negligible compared to the rest of the path. As we decrease the thickness of the slab, the pure planar excitation at 11.2 eV decreases in intensity leaving more visible the edge peak at $\sim 0.53\omega_p = 8.4$ eV in aluminum. All the losses have been normalized to the thickness of the slab in order to compare similar intensities. Because of the Begrenzungs effect, an increase in intensity in one excitation is linked to a decrease in another one. This is precisely the mechanism of intensity exchange between the planar and the edge excitation.

From these simulations of truncated slabs of aluminum, a characteristic loss function can also be inferred from the spectrum of losses. For perpendicular trajectories, the integration over the q component of the momentum broadens the excitation peaks, but the relevant distances remain valid since the effective contribution to the total integrated loss comes from parallel momentum components $q < \omega/v$. As we observed in the previous spectra, the coupling of modes is noticeable for slabs when $d < v/\omega_p$, i.e., slabs where d is thinner than about 15 nm in the case of aluminum. Therefore we assume slabs thicker than this relevant value in order to get the characteristic energy loss functions for the isolated edge and surface modes. For such a case, it is possible to check the influence of the edges in the spectrum of losses and develop a systematic way to include the corrections derived from their presence in a spectrum obtained experimentally. Under the conditions mentioned above, the characteristic energy loss function would be given by:

$$\frac{dP}{d\omega} = \frac{2e^2}{\pi\hbar v^2} L \left\{ \left[K_o\left(\frac{2\omega b}{v}\right) - \frac{A_1}{L} \right] \mathrm{Im}\left[\frac{-1}{0.5\varepsilon_{\mathrm{Al}} + (1-0.5)} \right] + \frac{A_2}{L} \mathrm{Im}\left[\frac{-1}{0.3\varepsilon_{\mathrm{Al}} + (1-0.30)} \right] \right\}, \tag{19}$$

where the coefficients A_1 and A_2 are dependent on the impact parameter b and for a 2-nm impact parameter are found to be $A_1 = 21.70$, $A_2 = 26.10$ nm. If the beam passed through the medium, the bulk term should be added as in expression (17), but for a trajectory outside the slab, there is no bulk contribution since the response function for vacuum is equal to zero. Notice that the excitation of the edge modes turns into a decrease in the excitation of the planar surface plasmon. These two contributions are constrained by the Begrenzungs effect and modify the planar contribution, which is linearly dependent on the sample size L. This is a useful first approximation to the whole spectrum but has two main limitations. The first one has already been pointed out and requires the study of sufficiently thick samples (which is the usual situation in electron microscopy). The second point is the fact that the exact spectrum is given by an infinite number of modes with their respective weights and here we only consider the most representative ones since the rest are negligible. The case of a slightly damped Drude-like metal is one of the most extreme examples to check this approximation since the loss spectrum shows well-defined and isolated peaks associated with each particular mode.

In practice, the modes do not appear so clearly separated and the approximation of the spectrum in terms of prominent modes is even better. For real materials such as MgO cubes this approximation is fulfilled very accurately.[26] Even for the Drude-like case, this few mode approximation is good enough when using a damping parameter $\gamma > \omega_p/20$ appropriate in most experimental situations. It is clear that the planar situation is a good approximation for slabs thicker than $\sim 10v/\omega_p$ (~ 150 nm in aluminum), but for thinner truncations it has been shown to be necessary to take into account the edge effect as a relevant feature modifying the spectrum of losses. For real materials with higher characteristic frequencies, the thickness for the validity of the planar approximation is not so big since this is again an extreme example of the edge effect. It is also possible to find out the range of impact parameters sensitive to the presence of the edge from a set of spectra for beams that penetrate the slab, but as we observed for the case of the isolated edge, this mode is more localized than the planar surface plasmon and one expects a similar behavior for the truncated slab, where the limit of the single slab is rapidly recovered. For the case of a cube, these results also give an indication of the circumstances in which it might be necessary to include the effects of 4 or more of the edges.

V. SITUATIONS INVOLVING THREE DIFFERENT MEDIA

For a system involving three or more media, the determinant giving the modes is obtained from $\Lambda(\omega) - [F_q]$, but now, $\Lambda(\omega)$ is given by the pair of dielectric functions ε_A and ε_B surrounding the particular interface l as shown in Eq. (2). Equation (8) is still valid for this case, but Eq. (9) has to be generalized with the additional index l to allow for the fact that $\Lambda(\omega)$ now has a subscript l depending on which media bound a particular segment of the interface. In that case Eq. (8) can be expressed for a system with n interfaces as

$$\sum_l^n \Lambda_l(\omega)[\sigma_q^l]_i^k = 2\pi\lambda_q^k[\sigma_q]_i^k, \tag{20}$$

where $[\sigma_q^l]_i^k$ is the q component of the interface charge density of the k mode, which is only valid at the ith point of the lth interface, and $[\sigma_q]_i^k$ is defined as in Eq. (9). If we project conveniently this expression over the interfaces according to Eq. (10), we get

$$\sum_l^n S_q^{k-l}\Lambda_l(\omega) = 2\pi\lambda_q^k. \tag{21}$$

In this latter expression, S_q^{k-l} takes account of a partial projection, since it is constrained to the l interface. In matrix notation S_q^{k-l} is found to be

$$S_q^{k-l} = \frac{\sum_i \sum_j \Delta\theta'^l_i \Delta\theta_j [\sigma_q^l]_i^k [\sigma_q]_j^k}{\sum_i \sum_j \Delta\theta'^l_i \Delta\theta_j [\sigma_q]_i^k [\sigma_q]_j^k}. \tag{22}$$

Once we get the kth eigenvalue λ_q^k of the interaction matrix and the values of S_q^{k-l} for the different interfaces labeled l, the mode position can be obtained from Eq. (21) for any group of dielectric functions pairs surrounding an arbitrary

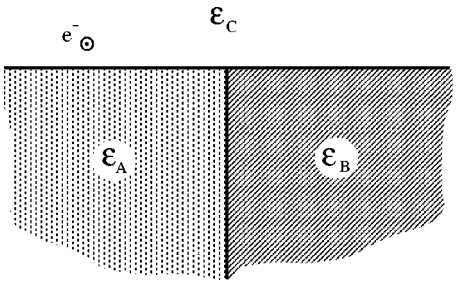

FIG. 8. Schematic representation of a *T* junction composed of three different media characterized by dielectric functions ε_A, ε_B, and ε_C.

number of interfaces forming a system. In this section, we analyze the particular case of a *T* junction formed by three different materials as an example of the application of the method. For such a system, the characteristic energy loss function is not so straightforward due to the coupling of different dielectric functions, as pointed out above, but anyhow, for some dominant modes, it may sometimes be possible to guess a loss function with a similar structure to the one presented in Eq. (16), where the values for the coefficients giving the mode frequency α_k are related to geometrical features of the problem. Here, we aim to throw light on these characteristic energy loss functions for real complex systems based on the exact numerical simulations performed with use of the boundary charge method.

A. *T* junction

The boundary charge method also allows the calculation of energy losses near junctions composed of three different media as shown, e.g., in Fig. 8. The three different dielectric functions characterizing the media involved are denoted by ε_A, ε_B, and ε_C and they will be taken as standard Drude-like functions where ω_{pA}, ω_{pB}, and ω_{pC} are the characteristic plasma frequencies. If we calculate the modes for such a system, the main feature to be pointed out is the presence of the planar modes corresponding to each pair of interfaces and which are given by $\varepsilon_A+\varepsilon_B=0$, $\varepsilon_A+\varepsilon_C=0$, and $\varepsilon_B+\varepsilon_C=0$. As for the edge or the truncated slab, it is possible to get the modes for such a structure by equating to zero the determinant of the interaction matrix $[F_q]$ in expression (7), corresponding to charge density oscillations with no external field. The calculation of modes for this case involving several media is more complicated than the case of a two-media system where the modes can be obtained independently of the composition of the material as was pointed out in Sec. II. In this case, the diagonalization of the matrix takes into account the mixing of different media in pairs [through $\Lambda_l(\omega)$] and the modes are strongly dependent on the composition of the structure.

A very interesting application of the boundary charge method in a three-component structure is the calculation of energy loss maps to compare with images obtained in energy-selected scanning transmission electron microscopy. As an example of this, we study the particular case of the structure of Fig. 8 where medium *A* is considered to be Al ($\omega_p=15.8$ eV; $\gamma=0.5$ eV), medium *B* is considered to be carbon ($\omega_p=23.5$ eV; $\gamma=1$ eV) and medium *C* is supposed to be vacuum. This choice was made to facilitate identification of the different modes. After diagonalizing the interaction matrix, a spread of modes is obtained. As in the edge and truncated slab cases, some modes are more relevant to the spectrum of losses than others. We have already pointed out the connection between the dominant mode positions and the space fraction filled by the materials. If we select the modes which are more prominent in terms of the intensity of the excitations, the first ones to be taken into account are the modes associated with the planar excitations at each boundary, i.e., $\varepsilon_{\mathrm{Al}}+\varepsilon_{\mathrm{C}}=0(\omega=20$ eV), $\varepsilon_{\mathrm{Al}}+1=0(\omega=11.17$ eV), and $\varepsilon_{\mathrm{C}}+1=0(\omega=16.6$ eV), which arise naturally in the method. Apart from these, we get other well-defined modes that can be excited at different ω values. In Figs. 9(a), 9(b), 9(c), and 9(d) we show energy-filtered loss spectra for some of the dominant modes both in a three dimensional plot as well as in a contour plot that can be directly compared with the filtered images obtained in a scanning microscope. The most interesting contour plot is the one at 14.5 eV, which is associated with charge density oscillations in the *T* junction itself. In fact, we conclude from calculations that the main features of the spectrum of losses are given by the peak at the junction and the three planar peaks along the three boundaries. By making an *ad hoc* assumption that the modes are still characterized by excitation functions $\mathrm{Im}\{-1/[\alpha\varepsilon_A+\beta\varepsilon_B+(1-\alpha-\beta)]\}$, we introduce a parameter β giving the position of the modes. We can show that this assumption, though certainly not rigorous, works moderately well. For the *T* junction shown in Fig. 8, where medium *A* fills 1/4 of space, *B* fills another 1/4 and half the space is vacuum, we may thus roughly guess the junction mode position by using an expression analogous to Eq. (16) with coefficients $\alpha_k=1/4$ and $\beta_k=1/4$. The energy value that fulfills the condition for the junction mode is $\omega=14.2$ eV, which agrees with the value obtained through the boundary charge method to an accuracy of 2%. In terms of this geometrical argument, if the three media junction were symmetric, i.e., each occupying an angle of $2\pi/3$, the value of the dominant mode position would be $\alpha_k=1/3$ and $\beta_k=1/3$, i.e., $\varepsilon_{\mathrm{Al}}+\varepsilon_{\mathrm{C}}+3=0$, and an ad hoc energy loss function characteristic of such a *T* junction could be computed with these values. If we include both the planar excitations and the junction excitation as the most relevant features of the losses, the expected approximate energy loss function for the system shown in Fig. 8, becomes

$$\frac{d^2P}{d\omega\,dz}=\frac{2e^2}{\pi\hbar v^2}\left\{A_1\,\mathrm{Im}\left[\frac{-1}{0.5\varepsilon_{\mathrm{Al}}+0.5\varepsilon_{\mathrm{C}}}\right]+A_2\,\mathrm{Im}\left[\frac{-1}{0.5\varepsilon_{\mathrm{Al}}+0.5}\right]+A_3\,\mathrm{Im}\left[\frac{-1}{0.5\varepsilon_{\mathrm{C}}+0.5}\right]+A_4\,\mathrm{Im}\left[\frac{-1}{0.25\varepsilon_{\mathrm{Al}}+0.25\varepsilon_{\mathrm{C}}+0.5}\right]\right\},\tag{23}$$

where the subscripts 1, 2, and 3 refer to the planar losses and the subscript 4 refers to the junction loss. The bulk term

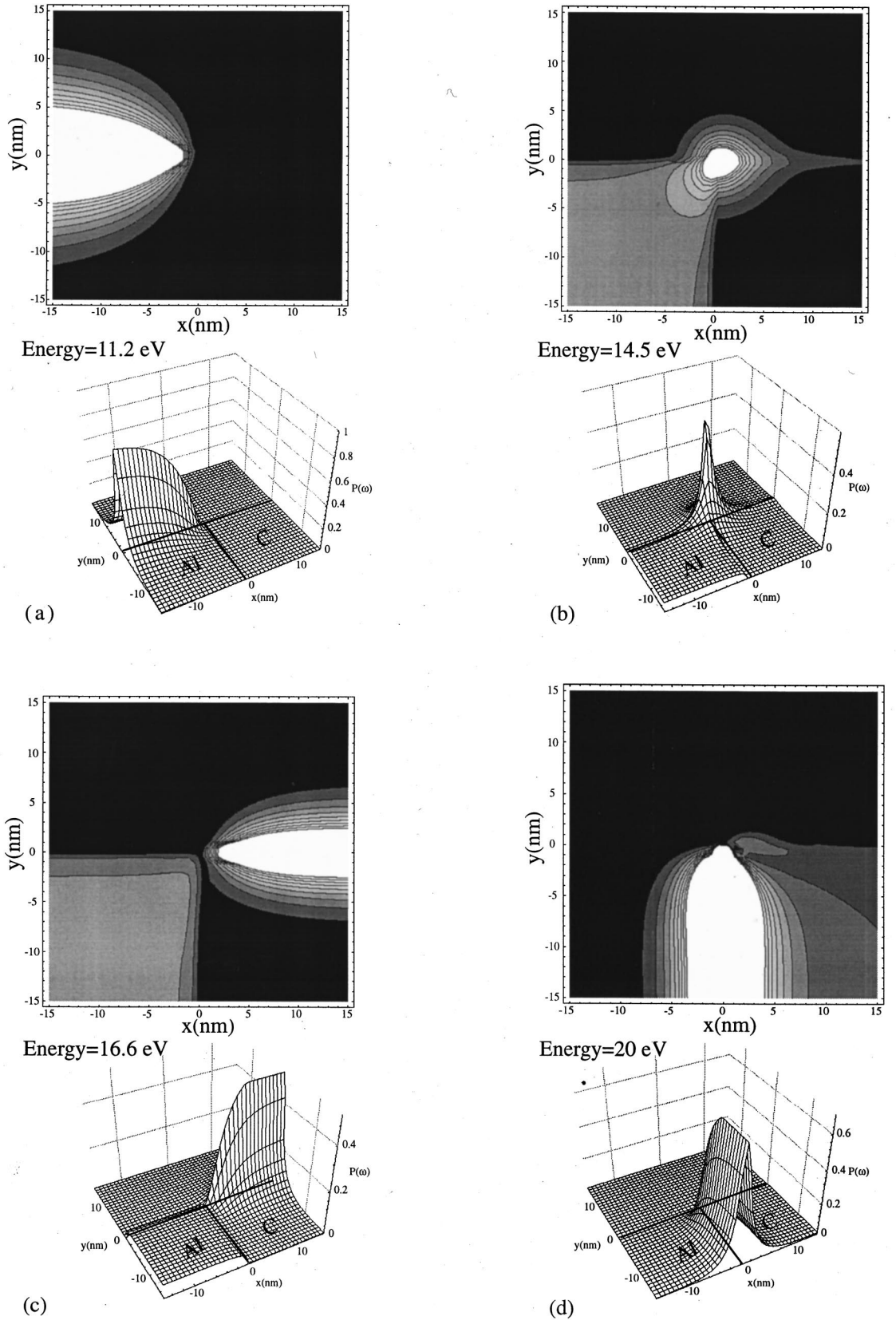

FIG. 9. (a), (b), (c), and (d) Simulation of filtered energy loss probability for the case of a 100 keV electron impinging on a T junction composed of aluminum ($\omega_p = 15.8$ eV, $\gamma = 0.5$ eV) and carbon ($\omega_p = 23.5$ eV, $\gamma = 1$ eV) next to vacuum. The values of the filtered energies are 11.2, 14.5, 16.6, and 20.0 eV, respectively and have been obtained through the diagonalization of the interaction matrix in the boundary charge method. The darker the region, the smaller the value of the probability of losing energy. Aluminum is contained in the region $x,y<0$, carbon for $x>0$, $y<0$ and vacuum for $y>0$.

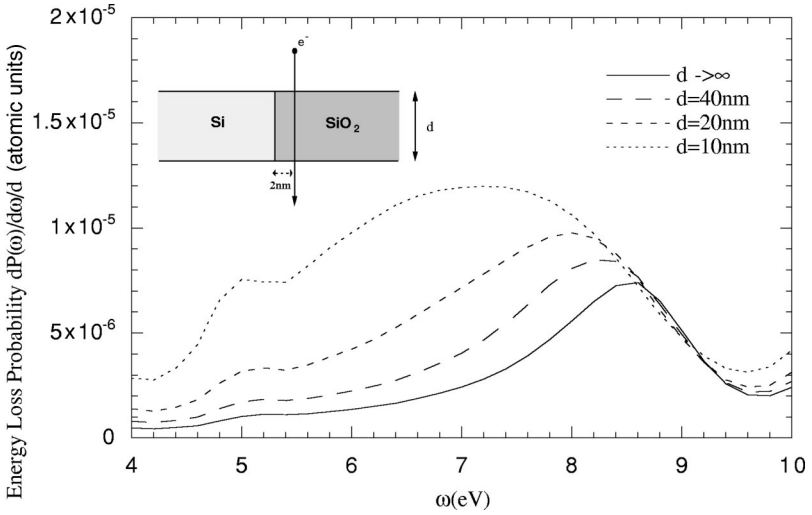

FIG. 10. Energy loss probability for a 100-keV electron traveling through a *I*-junction type geometry formed by Si and SiO_2 as shown in the inset. Spectra for different thickness of the film and a comparison with the infinite interface case are shown. In all the cases the impact parameter is 2 nm.

should be added when the trajectory crosses through aluminum or carbon. The dependence of the coefficients A_k with respect to the impact parameter is here even more complicated than in the two-media case, making clear the necessity of numerical simulations through, e.g., the boundary charge method to find the exact weight of the different excitations depending on the beam position.

Close investigation of the eigenvalue equation for the modes of the *T* junction indicates that they may be analytically related to the modes of the isolated edge, which were described in Sec. III. There is a possibility, which we plan to explore in a later publication, that this approach can also yield more exact excitation functions for the *T*-junction modes and eventually an improved form of Eq. (23). In the meantime we believe that this equation represents a useful working compromise.

B. Si-SiO_2 *I* junction

The most important practical case to test the success of the boundary charge method is the complex but realistic structure of the *I* junction often encountered in experiments. This comprises a thin slab containing two different dielectric regions separated by a boundary running normal to the slab surfaces. We study a system composed of silicon (Si) and silica (SiO_2) when the electron beam penetrates one of the two regions [see Fig. 10]. Besides the bulk plasmon of the material penetrated, the Si-SiO_2 interface plasmon given by the relation $\varepsilon_{\mathrm{Si}}+\varepsilon_{\mathrm{SiO_2}}=0$ is also excited. The exact position of this interface plasmon peak has been recently studied relativistically and good agreement with experiments has been achieved for thick enough slabs (180 nm thick) where the planar interface approximation can properly be used.[23] As in previous sections, it is possible to estimate the influence of the thickness of the slab on the weight and position of this interface plasmon and the relevant thicknesses at which the edges and the coupling between surfaces should be taken into account. The experimental situation for such a junction is represented in the insert in Fig. 10 where the beam travels through the SiO_2 with a 2-nm impact parameter. We constrain our study to small impact parameters in order to reduce the influence of retardation in the position of the peak. The spectrum of losses for different slabs is represented to Fig. 10 both for the range of validity of the planar approximation ($d\rightarrow\infty$) and for thin slabs where the edge effect shifts the peak downwards. From the simulations in the figure, one can establish that the planar approximation is very good for slabs thicker than ~ 50 nm but fails when dealing with thinner ones. Although we will return to this point later, it is convenient now to study the problem in terms of relevant thicknesses and characteristic losses, which can throw light on the effect. The case we present here is more complicated to study due to the complex dielectric response functions characterizing both media. In the case of a Drude-like truncated slab, we were able to analyze well-defined and separate losses associated with the particular modes in a system, but for a realistic case, such as this one, it is not possible to identify the contribution of each mode in such a clear way. Nevertheless, as for the case of the truncated slab, the downward shifting can be interpreted in terms of excitation of edge modes whose relative intensity is more noticeable as the thickness of the slab decreases. As in the case of the truncated slab, we can also distinguish here three different regions in order to interpret the Si-SiO_2 interface plasmon peak position and intensity: for slabs thicker than $\sim 10v/\omega_p$, (~ 50 nm for this case) a treatment based on the planar interface approximation is sufficient to deal with the energy losses. For slabs thinner than this value, the presence of the junctions is clearly noticeable and new junction modes given by the relation $\varepsilon_{\mathrm{Si}}+\varepsilon_{\mathrm{SiO_2}}+2=0$ ($\alpha_k=1/4$, $\beta_k=1/4$), must be included in the spectrum of losses. Finally, in the case of very thin slabs ($d<v/\omega_p<5$ nm), the coupling of edges and interfaces, gives rise to new surface modes in the case of very thin films and makes it difficult to express the losses in terms of well-defined excitations. The contribution of different values of the parallel momentum component q also broadens the peak for trajectories perpendicular to the axis of symmetry, since it takes into account contributions of differently coupled modes to the spectra of losses. In any case, the final intensity is mainly given by very low components of the momentum close to the value ω/v. In a first approximation, for slabs greater than 5 nm in the case of SiO_2, it is possible to express the losses for the case of a 100-keV electron im-

pinging on a junction as shown in the inset of Fig. 10 in terms of the weighted modes as follows:

$$\frac{dP}{d\omega}=\frac{2e^2}{\pi\hbar v^2}L\left\{A_o\left[\frac{-1}{\varepsilon_{SiO_2}}\right]+A_1\,\mathrm{Im}\left[\frac{-1}{0.5\varepsilon_{SiO_2}+0.5}\right]\right.$$

$$+A_2\,\mathrm{Im}\left[\frac{-1}{0.5\varepsilon_{Si}+0.5\varepsilon_{SiO_2}}\right]$$

$$\left.+A_3\,\mathrm{Im}\left[\frac{-1}{0.25\varepsilon_{Si}+0.25\varepsilon_{SiO_2}+0.5}\right]\right\},\qquad(24)$$

The first mode (labeled 0) corresponds to the SiO_2 bulk plasmon, the surface modes labeled 1 (SiO_2-vacuum), and 2 (Si-SiO_2 interface) correspond to the pure planar cases and the last one (labeled 3) corresponds to the *T*-junction edge mode characterized by $\alpha_k=0.25$, $\beta_k=0.25$ as obtained before. The coefficients $A_k=A_k(b,\omega)$, are dependent on the impact parameter and the thickness L of the slab. For the energy range (4–10 eV), it is adequate to take the last two modes (labeled 2 and 3 in the characteristic loss function) to simulate the main features of the spectrum since the SiO_2-vacuum interface peak and the Si and SiO_2 bulk plasmon peaks appear at 18 and 23 eV, respectively. In this range of losses, the single slab relation, $A_o=\ln(k_cv/\omega)-0.5A_1$ and $A_1=\mathrm{const}/L$ of the type employed in Eq. (19) can then be used.[1] For the case of a trajectory penetrating Si, the characteristic energy loss function can be obtained by interchanging SiO_2 with Si in expression (24). With optical dielectric data for amorphous SiO_2 and crystalline Si,[27] the interface peak appears at 8.6 eV from $\varepsilon_{Si}+\varepsilon_{SiO_2}=0$ and the junction edge mode appears at 7.6 eV from $\varepsilon_{Si}+\varepsilon_{SiO_2}+2=0$. Since both modes are very close together in the spectrum and are broadened by damping, we simply observe a shifting from one value (8.6 eV) to another (7.6 eV) as we decrease the slab thickness, instead of two separate modes, weighted according to the sample thickness as in Fig. 7. From this point of view, it is possible now to understand the spectra in Fig. 10, where numerical calculations for the energy loss probability per eV normalized to the slab thickness are provided for a 100-keV electron beam traveling at 2 nm from the interface separating both media. As pointed out, there is 1 eV shift of the interface plasmon peak, which should be detectable in thin enough films when using high resolution in STEM. If we split the peak into two different contributions according to the peaks in the characteristic loss function in expression (24), A_2 and A_3 can be expressed for a fixed impact parameter, in an analogous way to the truncated slab case [see Eq. (18)], i.e., $A_2=K_o(2\omega b/v)-\mathrm{const}_2/L$ and $A_3=\mathrm{const}_3/L$ where $\mathrm{const}_2=19.8$ nm and $\mathrm{const}_3=21.7$ nm for the case of 2 nm impact parameter. Notice that these values are coincident with those obtained for the case of the truncated slab and have the same meaning: they are fixed contributions of the edge effect independent of the thickness of the slab that modify the usual $[K_o(2\omega b/v)]$ term proportional to the thickness. On the other hand, for the isolated edge, it is also possible to guess a dependence of these coefficients on the impact parameter *b*, by introducing an exponential decay for the plasmon intensity, which depends on the nature of the surface plasmon $[A_k(b,\omega)\sim\exp(-n\omega b/v)]$ where *n* depends on the particular mode). The modes associated to the edges and junctions are more localized than the planar ones therefore, one expects the parameter *n* to be greater for these modes.

For very thin films, the main effect influencing the spectrum of losses is the coupling among surfaces and edges, as pointed out for the case of the truncated slab in Sec. IV. For the case of the Si-SiO_2 junction, the relevant thickness parameter below which the coupling is significant is 5 nm. In practice, it is very difficult to deal with such thin films, therefore we constrain our study to values greater than this relevant parameter. Below these values, the structure of the modes complicates as can be seen in Fig. 4.

VI. CONCLUSIONS

We have studied complex systems whose normal modes and characteristic energy loss functions can only be handled successfully by numerical calculations. The complexity of the systems arises from the presence of sharp edges and junctions such as the truncated slab or the junctions composed from more than two media. The method employed here establishes a systematic procedure to express the losses in terms of excitation of modes, which are given by the geometry of the system. We have obtained general quantitative criteria to deal with the edge effect at truncations, cubes or junctions in slabs where we distinguish three different cases. For interfaces longer in the beam direction than $\sim 10v/\omega_p$, the planar approximation treats successfully the intensity and position of the losses since the edge effect is negligible in comparison with the planar interface loss. For truncated interfaces between v/ω_p and $\sim 10v/\omega_p$, the edge effect has to be taken into account via the presence of the dominant new excitation associated with the edge itself as well as through the decrease of intensity (Begrenzungs effect) of well-known excitations such as bulk and planar surface plasmons. For this range of structures, an approximation directly related to the geometry has been proved to be adequate to express the characteristic energy loss functions in terms only of the dominant modes. The third range of sizes belongs to the case of structures with truncations smaller than v/ω_p, where only the numerical simulations based on, e.g., the boundary charge method developed here, can adequately describe the complex coupling of modes and the resulting loss spectrum.

ACKNOWLEDGMENTS

The authors would like to thank Iberdrola for support (A.H.) and the Departamento de Educación, Universidades e Investigación of the Basque Country Government for supporting the visit to the Cavendish Laboratory through its predoctoral grants program (J.A.) (Project No. PI 1997/39).

*Permanent address: Department of Applied Physics, Chalmers University of Technology, 412 96 Göteborg, Sweden.
[1] R. H. Ritchie, Phys. Rev. **106**, 874 (1957).
[2] P. M. Echenique and J. B. Pendry, J. Phys. C **8**, 2936 (1975).
[3] P. E. Batson, Ultramicroscopy **9**, 277 (1982).
[4] T. L. Ferrell and P. M. Echenique, Phys. Rev. Lett. **55**, 1526 (1985).
[5] P. M. Echenique, A. Howie, and D. J. Wheatley, Philos. Mag. B **56**, 335 (1987).
[6] N. Zabala, A. Rivacoba, and P. M. Echenique, Surf. Sci. **209**, 465 (1989).
[7] C. Walsh, Philos. Mag. **59**, 227 (1989).
[8] L. Dobrzynski and A. A. Maradudin, Phys. Rev. B **6**, 3810 (1972).
[9] L. C. Davis, Phys. Rev. B **14**, 5523 (1976).
[10] D. Langbein, J. Phys. A **9**, 627 (1976).
[11] N. Zabala and A. Rivacoba, Phys. Rev. B **48**, 14 534 (1993).
[12] J. Aizpurua, A. Rivacoba, and S. P. Apell, Phys. Rev. B **54**, 2901 (1996).
[13] J. Q. Lu and A. A. Maradudin, Phys. Rev. B **42**, 11 159 (1990).
[14] R. Ruppin, Z. Phys. D **36**, 69 (1996).
[15] R. Fuchs, Phys. Rev. B **11**, 1732 (1975).
[16] F. Ouyang and M. Isaacson, Philos. Mag. B **60**, 481 (1989).
[17] F. Ouyang and M. Isaacson, Ultramicroscopy **31**, 345 (1989).
[18] F. J. García de Abajo and J. Aizpurua, Phys. Rev. B **56**, 15 873 (1997).
[19] L. D. Marks, Solid State Commun. **43**, 727 (1982).
[20] J. M. Cowley, Surf. Sci. **114**, 587 (1982).
[21] R. H. Milne and P. M. Echenique, Solid State Commun. **55**, 909 (1985).
[22] M. Walls and A. Howie, Ultramicroscopy **28**, 40 (1989).
[23] P. Moreau, N. Brun, C. A. Walsh, C. Colliex, and A. Howie, Phys. Rev. B **56**, 6774 (1997).
[24] F. J. García de Abajo and A. Howie, Phys. Rev. Lett. **80**, 5180 (1998).
[25] S. P. Apell, P. M. Echenique, and R. H. Ritchie, Ultramicroscopy **65**, 53 (1996).
[26] J. Aizpurua, B. Rafferty, F. J. de Abajo, and A. Howie, Inst. Phys. Conf. Ser. **153**, 277 (1997).
[27] *Handbook of Optical Dielectric Constants of Solids*, edited by D. Palik (Naval Research Laboratory, Washington, D.C., 1985).